Numerical Simulation of Sloshing Motion inside a Two Dimensional Rectangular Tank by Level Set Method

Abstract

Purpose – This research aims to develop the numerical simulated methodology for sloshing motion of fluid inside a two dimension rectangular tank, and parametric studies were performed for three parameters - excitation frequency, excitation amplitude, and liquid depth.

Design/methodology/approach – In this study, a numerically simulated methodology by using the cell-centered pressure-based SIMPLE scheme and level set method for the sloshing motion of fluid in a rectangular tank has been developed. The convection term in the Navier-Stokes equations and the equations used in the level set method were treated by the second-order upwind scheme. The temporal derivative terms were solved by the three-level second order scheme. The diffusion term in the Navier-Stokes equations alone was solved by the central-difference scheme. All algebraic equations in this study were solved by the point Gauss-Seidel method. A fully implicit scheme to treat the level set distancing equation, written as the advection equation, was developed in this study. In addition, the level set distancing equation was solved by the iterative procedure to determine the variation of free surface.

Findings – For given excitation amplitude together with a liquid depth, the free surface displacement increases when the excitation frequency is less than the resonance frequency of tank. However, the free surface displacement decreases when the excitation is greater than the resonant frequency of the tank. It is noted that the maximum free surface displacement is generated under the circumstance for which the excitation frequency approaches the resonant frequency. The excitation amplitude and the excitation frequency have a substantial effect on the impact pressure on the wall of the tank being investigated.

Originality/value – The sloshing motion of fluid in a rectangular tank has been studied by researchers and scholars using many numerical methods; however, literature employing the level set method to study the sloshing motion of fluid is limited. In this study, the cell-centered pressure-based SIMPLE scheme and level set method can be employed to predict the sloshing motion. The numerical methodology can help the engineer to predict sloshing motion of fluid.

1. Introduction

When a tank is subject to oscillation in a direction, wave motion of the liquid takes place in the partially-filled tank. This phenomenon is called sloshing. The ship which transports oil or liquefied natural gas oscillates by ocean waves. As a result of the sloshing motion by the motion of ship, the oil or liquefied natural gas in the storage tank is exited. If the resonant frequency of liquid sloshing is coherent with that of the ship, the ship could be toppled and sunk in the ocean. With the fuel storage tank occupying the bulk volume of the rocket powered by liquid propellant, vibration of flying vehicle leads to sloshing motion of the liquid fuel in the tank. More violent sloshing motion could affect the stability of vehicle which in turn affects the trajectory of vehicle. In order to reduce the sloshing motion, baffles are installed in the fuel storage tank to enhance the stability of a flying vehicle.

From the mathematical point of view, the sloshing motion is a difficult problem to analyze. The boundary condition of the free surface is nonlinear, and the position of free surface varies with time and position. As a result, it is difficult to develop the analytical solution for sloshing motion. Many scholars use the potential flow theory to build the mathematical model, with the kinematic boundary condition and dynamic boundary condition applied on the free surface (Nakayama and Washizu 1980 and 1981, Wu et al. 1998, Cho and Lee, 2004 and 2005, Wang and Khoo 2005, Biswal et al. 2006, Sriram et al. 2006, Firouz-Abadi et al. 2008). It is noted that the velocity potential is a primitive variable and the position of free surface is obtained by kinematic boundary conditions. Both finite element method and boundary element method have been used to solve the Laplace equation. As mentioned above, small free surface displacement can be predicted by finite element method and boundary element method. When more violent sloshing motion is excited by the external excitation with frequency of external excitation near the natural frequency of sloshing motion, finite element method and boundary element method cannot be used in this case. However, Arbitrary Lagrangian-Eulerian (ALE) method and Lagrangian finite element method have been employed to solve the Navier-Stokes equations for sloshing motion (Okamoto and Kawahara 1990, Ramaswamy et al. 1986). In these methods, computational grid has to be regenerated at each time step. It is noted that for substantial deformation of free surface, such as overturning flow or breaking wave, these methods cannot be used.

The finite difference method and coordinate transformation method have been successfully applied on solving the sloshing motion (Frandsen 2003, Chen et al. 2005 and 1999). In many numerical studies, the physical domain is transformed into computational domain by a specific mathematical

function or specific functions. After using the coordinate transformation method, the finite difference method can be employed to solve the governing equations. In this case, the breaking wave inside the tank cannot be predicted because the numerical grid cannot be separated.

In recently research, interfacial capture methods have been carried out to predict sloshing motion. In interfacial capture methods, the computational grid is fixed; the variation of free surface is predicted by solving scalar function. Two interfacial capture methods are applied to capture the variation of free surface – Level Set Method (LSM) (Osher and Sethian 1988) and Volume of Fluid (VOF) Method (Hirt and Nichols 1986). In the VOF method, the volume fraction of cell is a primitive variable. Volume fraction of cell represents the fraction of cell occupied by liquid, with 1 – (volume fraction) by gas. It is necessary to use the iteration procedure to solve the volume fraction. After solving the volume fraction, the free surface can be constructed by using the geometry reconstruction method (Young 1982, Noh and Woodard 1976, Hirt and Nichols 1986). For level set method, the level set function φ is a primitive variable. The locus of free surface can then be determined by the level set function. Through the finite volume method or finite difference method in solving the level set function, the variation of free surface can be evaluated. The detailed descriptions about VOF method and LSM can be obtained from the papers cited in this paragraph. For finite difference method and finite volume method, the computer resource required is much larger than that needs by the boundary element method, and the effort of mesh generation for these two methods is more extensive than that needs by either the boundary element method or the Smooth Particle Hydrodynamics (SPH) method. In interfacial capture methods, breaking wave and overturning flow are easily predicted.

It is noted that in this study, the iterative procedure used by the level set method doesn't need to account for the geometry reconstruction. After solving the Navier-Stokes equations together with the equation used in the level set method, the velocity of fluid and variation of free surface can be obtained. The level set method has been successfully applied to solve the problem of dam break (Yue 2003, Marchandise 2006) as well as the problem associated with violent sloshing motions (Chen, 2009).

Recently, the SPH method has been applied to solve the violent sloshing motion with large free surface displacement (Iglesias 2004 and 2006, Delorme et al. 2009). The fluid is represented by the set of particles. These particles follow the fluid motion. This method doesn't need to account for the mesh generation. The SPH method can predict sloshing motion for the cases with large amplitude of free surface and large frequency of surge excitations. In the SPH method, the pressure is obtained by equation of state. The pressure peak could be overestimated by the SPH method (Delorme, 2009).

This study was aimed to develop a numerical model for solving the two-dimensional sloshing motion. The viscous fluid flow theory was adopted to build up mathematical model. The level set method was then used to predict the behaviour of free surface. For numerical method, the finite volume method was used to solve the governing equations, and fully implicit scheme was used to treat the level set method.

2. Mathematical Model

The problem under consideration is sloshing motion in a two-dimensional rectangular tank. As shown in Fig. 1, the tank has a width L and a height H, and the tank is filled with liquid to a depth h. As shown in Fig. 2, the non-inertia rectangular coordinate system is adopted to construct the governing equation for sloshing motion.

The coordinate system $O'X'Y'Z'$ is fixed on the rigid tank and the other coordinate system $OXYZ$ is associated with the stationary coordinate system. The tank is forced to move in the x direction and y direction and is forced to pitch about the origin O with an angular velocity $\Omega(t)$.

In order to construct the governing equations, the following assumptions were made:

1. The fluid is Newtonian.
2. The fluid flow is incompressible and laminar.
3. All fluid properties are assumed to be unchanged with time.
4. The surface tension of fluid is neglected because that the Bond number is much larger than unity.

According to the non-inertia rectangular coordinate system and the above assumptions, the governing equations for sloshing motion can be expressed as follows:

$$\int_V \rho \vec{V} \cdot \vec{n} dA = 0 \tag{1}$$

$$\frac{\partial}{\partial t}\int_V \rho \vec{V} dV + \int_s \rho \vec{V}\vec{V} \cdot \vec{n} dA = -\int_s p\vec{n} dA + \int_s \mu\left(\nabla \vec{V} + \nabla \vec{V}^T\right) \cdot \vec{n} dA + \int_V \rho \vec{f} dV \tag{2}$$

$$\vec{f} = \vec{g} - \frac{d\vec{U}}{dt} - \alpha \times \vec{r} - 2\Omega \times \vec{V} - \Omega \times (\Omega \times \vec{r}) \tag{3}$$

Eq. (1) is the continuity equation and eq. (2) is the momentum equation. The last term of eq. (2) is

the external force acting on the rectangular tank and the external force is expressed by eq. (3). In eq. (1) and eq. (2), ρ is the density of fluid, p is pressure of fluid, $\vec{V}$ is velocity of fluid, and $\vec{n}$ is normal vector of interface. In eq. (3), $\vec{g}$ is the gravitational acceleration, $\vec{U}$ is velocity of the rectangular tank, $\vec{r}$ is position vector of the fixed coordinate system of tank, α is the angular acceleration of tank and Ω is angular velocity of tank.

In the level set method, the free surface is defined as the one with a level set function $\varphi = 0$. The level set method is often expressed as advection equation so that this equation is expressed as follows:

$$\frac{\partial \varphi}{\partial t} + \vec{V} \cdot \nabla \varphi = 0 \tag{4}$$

where $\vec{V}$ is the local fluid velocity which is obtained from eq. (2). The sharp discontinuity on density and viscosity causes a numerical instability when eq. (4) is solved. In order to avoid numerical instability, the narrow transition zone is constructed around the free surface to redefine the density and viscosity on the narrow transition zone. For the density and viscosity in the transition zone, Colicchio et al. (2005) proposed the formulas of the density and viscosity to redefine these two quantities. The formula of density and viscosity are defined as follows:

$$\rho(\varphi) = \begin{cases} \rho_l & \text{if } \left(\varphi - \delta_\rho c\right) < -\delta_\rho \\ \sqrt{\rho_l \rho_g}\exp\left[\frac{1}{2}\log\left(\frac{\rho_l}{\rho_g}\sin\frac{\pi}{2\delta_\rho}\left(\varphi - \delta_\rho c\right)\right)\right] & \text{if } \left|\varphi - \delta_\rho c\right| < \delta_\rho \\ \rho_g & \text{if } \left(\varphi - \delta_\rho c\right) > \delta_\rho \end{cases} \tag{5}$$

$$\frac{1}{\mu}(\varphi) = \begin{cases} \mu_l^{-1} & \text{if } \varphi < -\delta_\mu \\ \frac{\mu_l^{-1} - \mu_g^{-1}}{2}\left(\frac{\sin\left(\pi\varphi/\delta_\mu\right)}{\pi} - \frac{\varphi}{\delta_\mu}\right) + \frac{\mu_l^{-1} + \mu_g^{-1}}{2} & \text{if } |\varphi| < \delta_\mu \\ \mu_g^{-1} & \text{if } \varphi > \delta_\mu \end{cases} \tag{6}$$

In this study, density and viscosity in the transition zone are defined by eq. (5) and eq. (6).

Eq. (4) is a nonlinear hyperbolic equation and the initial condition for eq. (4) can be defined as a sign distance function,

$$\varphi = \begin{cases} -d & for \;\; X \in \Omega_{\text{gas}} \\ 0 & for \;\; X \in \Gamma(free\ surface) \\ d & for \;\; X \in \Omega_{liquid} \end{cases} \tag{7}$$

In eq. (7), d is the normal distance between the nodal point and free surface. However, eq. (4) cannot preserve as a sign distance function as time proceeds, and the transition zone will be changed at the next time step. In order to preserve the sign distance function and redefine the transition zone, one can perform the re-initialization (or re-distancing) procedure to define the sign distance function and transition zone at each time step.

The re-initialization procedure can be obtained by solving eq. (8); the equation can be expressed as follows:

$$\frac{\partial d}{\partial \tau} + sign(\varphi)\left(|\nabla d| - 1\right) = 0 \cdot \tag{8}$$

The initial condition for eq. (8) is as follows:

$$d(\vec{x}, 0) = \varphi(\vec{x}, t) \tag{9}$$

In this study, eq. (8) is called level set distancing equation. It is noted that eq. (8) can be solved by the iterative procedure. Once the numerical solution approach to the steady solution is done, one can complete the re-distancing procedure and then advance to next time step.

As above, the governing equations of sloshing motion are equations (1), (2), (3), (4), and (8). The fluid properties are based on equations (5) and (6). To develop numerically simulated methodology, the governing equations of sloshing motion can be written by using dimensionless variables. These dimensionless variables are expressed as follows:

$$\vec{V}^* = \frac{\vec{V}}{\sqrt{gL}} \quad p^* = \frac{p}{\rho_l g L} \quad x^* = \frac{x}{L} \quad y^* = \frac{y}{L} \quad z^* = \frac{z}{L} \quad t^* = t\sqrt{\frac{g}{L}} \quad \vec{r}^* = \frac{\vec{r}}{L} \quad \vec{U}^* = \frac{\vec{U}}{\sqrt{gL}} \quad \rho^* = \frac{\rho}{\rho_l}$$

$$\varphi^* = \frac{\varphi}{L} \quad \Omega^* = \frac{\Omega}{2\pi}\sqrt{\frac{L}{g}} \quad \alpha^* = \frac{\alpha}{2\pi}\frac{L}{g} \tag{10}$$

By substituting dimensionless variables into the governing equations, the dimensionless form of governing equations can be expressed as follows:

$$\int_s \rho^* \vec{V}^* \cdot \vec{n} dA = 0 \tag{11}$$

$$\frac{\partial}{\partial t^*}\int_V \rho^* \vec{V}^* dV + \int_s \rho^* \vec{V}^* \vec{V}^* \cdot \vec{n} dA = -\int_s p^* \vec{n} dA + \frac{1}{\mathrm{Re}_L}\int_s \left(\nabla \vec{V}^* + \nabla \vec{V}^{*T}\right)\cdot \vec{n} dA + \int_V \rho^* \vec{f}^* dV \tag{12}$$

$$\vec{f}^* = \frac{1}{Fr} - \frac{d\vec{U}^*}{dt^*} - 2\pi\alpha^* \times \vec{r}^* - 4\pi\Omega^* \times \vec{V}^* - 4\pi^2 \Omega^* \times \left(\Omega^* \times \vec{r}^*\right) \tag{13}$$

$$\frac{\partial \varphi^*}{\partial t^*} + \vec{V}^* \cdot \nabla \varphi^* = 0 \tag{14}$$

where $\mathrm{Re}_L = \frac{\rho_l V_\infty L}{\mu_l}$, $Fr = \frac{V_\infty}{\sqrt{gL}}$, V_∞ is the characteristic velocity, and L is the characteristic length. In this study, the characteristic velocity is $\sqrt{gL}$. In the next section, the numerical discretization schemes to evaluate the governing equations are discussed.

3. Numerical Method

In this study, the finite volume method was employed to solve the governing equations. All of variables were defined at the center of the cell. The second-order upwind scheme was adopted to discretize the convection term, and the central difference scheme was used to discretize the diffusion term. The three-level second order scheme (Ferziger and Peric 2002) was employed to discretize the temporal derivative term. In addition, the momentum interpolation method proposed by Rhie and Chow (1983) was used to avoid the checkerboard error. Numerical solutions of velocity and pressure associated with the fluid flow of the sloshing motion were done by the cell-centered pressure-based SIMPLE scheme described by Chen (2005).

3.1 Discretization of Level Set Method

For level set method, the spatial derivative term in eq. (14) is treated by the second-order upwind scheme. As shown in Fig. 3, the level set function on the cell face is approximated by the Taylor series expansion. The Taylor series expansion for level set function is as follows:

$$\varphi^{LHS} = \varphi_{p1} + \left.\frac{\partial \varphi}{\partial x}\right|_{p1}\left(x_c - x_{p1}\right) + \left.\frac{\partial \varphi}{\partial y}\right|_{p1}\left(y_c - y_{p1}\right) + HOT \tag{15}$$

$$\varphi^{RHS} = \varphi_{p2} + \left.\frac{\partial \varphi}{\partial x}\right|_{p2}\left(x_c - x_{p2}\right) + \left.\frac{\partial \varphi}{\partial y}\right|_{p2}\left(y_c - y_{p2}\right) + HOT \tag{16}$$

$$\varphi_f = \frac{1}{2}\left(\varphi^{RHS} + \varphi^{LHS}\right) - \frac{1}{2} sign\left(1, \dot{m}_f\right)\left(\varphi^{RHS} - \varphi^{LHS}\right) \tag{17}$$

In equations (15) and (16), $\frac{\partial \varphi}{\partial x}$ and $\frac{\partial \varphi}{\partial y}$ are the gradients of level set function at the cell center; the gradients of level set function at the cell center can be evaluated by the Gauss's divergence theorem as follows:

$$\int_V \frac{\partial \varphi}{\partial x_i} dV = \int_A \varphi n_i dA, \quad \frac{\partial \varphi}{\partial x_i} \approx \frac{\sum_{k=1}^{N_{face}} \varphi_f n_{i,k} A_k}{\Delta V}. \tag{18}$$

The temporal derivative term in eq. (14) is approximated by using three-level second order scheme. After the numerical discretization, Eq. (14) is expressed as an algebra equation as follows:

$$a_{\phi,p}\Delta\varphi_p = \sum_{nb} a_{nb}\Delta\varphi_{nb} + RHS_\varphi \tag{19}$$

where $a_{p1} = \max(-\dot{m}_f, 0)$, $a_{p1} = \max(\dot{m}_f, 0)$, $a_p = \sum_{nb} a_{nb} + \frac{3(\Delta\varphi)^m \Delta V}{2\Delta t}$, and

$$RHS_\varphi = -\sum_{i=1}^{N_{face}} \dot{m}_i \varphi_i^n + \frac{\left(\varphi^n - \varphi^{n-1}\right)\Delta V}{2\Delta t} - \frac{3\left(\left(\varphi^{n+1}\right)^m - \varphi^n\right)\Delta V}{2\Delta t}$$

Eq. (19) is then calculated by the point Gauss-Seidel method. It is noted that φ^* is obtained from eq. (20) below:

$$\varphi^* = \varphi^n + \Delta\varphi. \tag{20}$$

In this study, φ^* is viewed as the variation of free surface. In the sloshing motion, the free surface is changed by velocity of fluid and external excitation source. Different angular frequency is set to excite the rectangular tank; the value of φ^* can be obtained from equations (19) and (20). The

value of φ^* is recorded during each iteration procedure to trace the variation of free surface.

3.2 Re-initialization Procedure

To ensure that the value of φ^* satisfies eq. (7), eq. (8) needs to be used for the re-initialization procedure. Many scholars have proposed numerous methods to solve eq. (11), such as Russo and Smereka (2000) and Hartmann et al. (2008). In this study, a new methodology of re-initialization scheme is derived as follows.

In order to develop the implicit scheme, eq. (8) is written as follows:

$$\frac{\partial d}{\partial \tau} + sign(\varphi)\frac{\nabla d}{|\nabla d|}\cdot\nabla d = sign(\varphi), \tag{21}$$

where $sign(\varphi)\nabla d / |\nabla d|$ is treated as a characteristic velocity; the primitive variable d is expressed as follows:

$$d = d^* + \Delta d \tag{22}$$

By substituting eq. (22) into eq. (21), eq. (21) is expressed as follows:

$$\frac{\partial(\Delta d)}{\partial \tau} + sign(\varphi)\frac{\nabla d}{|\nabla d|}\cdot\left[\nabla(\Delta d)\right] = -sign(\varphi)\left(\frac{\nabla d}{|\nabla d|}\cdot\nabla d - 1\right). \tag{23}$$

In eq. (22), d^* is the intermediate value obtained from the iteration process, and Δd is the correction of d^*. The solution of Δd is used to update the value of d^*, and iterations are performed until the right-hand side of eq. (23) approaches zero, leading to the condition where $|\nabla d| = 1$.

As shown in Fig. 4, the value of φ near the free surface (where $\varphi = 0$) has opposite sign so that $\varphi_{p1}^0 \varphi_{p2}^0 < 0$. Usually, methods used to solve eq. (21) are the upwind scheme, where the discrete derivatives are determined by the upwind difference scheme according to the direction of the characteristic. However, the discontinuity on the free surface is not desirable for upwind difference scheme and should be avoided. In this study, the value of d_{ij}^{n+1} near the free surface is treated as follows:

$$d_{ij}^{n+1} = sign\left(\varphi^0\right) D_{ij} \tag{24}$$

where $D_{ij} = \left| \dfrac{d_{ij}^0}{\sqrt{\left(\dfrac{\partial d_{ij}^0}{\partial x}\right)^2 + \left(\dfrac{\partial d_{ij}^0}{\partial y}\right)^2}} \right|$.

Near the free surface, $\frac{\partial d_{ij}^0}{\partial x}$ and $\frac{\partial d_{ij}^0}{\partial y}$ are evaluated by eq. (25) and eq. (26) below:

$$\frac{\partial d_{ij}^0}{\partial x} = \frac{1}{2}\left(\frac{\partial d_{p1}^0}{\partial x} + \frac{\partial d_{p2}^0}{\partial x}\right), \quad \frac{\partial d_{ij}^0}{\partial y} = \frac{1}{2}\left(\frac{\partial d_{p1}^0}{\partial y} + \frac{\partial d_{p2}^0}{\partial y}\right) \tag{25}$$

As shown in Fig. 5, subscripts P_1 and P_2 in equations (25) are the nodal points. $\frac{\partial d_{p1}^0}{\partial x}$ and $\frac{\partial d_{p1}^0}{\partial y}$ are obtained by equations (26) and (27) below:

$$\begin{aligned} &a_+ = \max(a, 0), a_- = \min(a, 0), b_+ = \max(b, 0), b_- = \min(b, 0) \\ &c_+ = \max(c, 0), c_- = \min(c, 0), d_+ = \max(d, 0), d_- = \min(d, 0) \end{aligned} \tag{26}$$

$$\frac{\partial d_{p1}^0}{\partial x} = \begin{cases} \max\left(a^+, b^-\right) \text{ if } \varphi_{p1}^0 > 1, \\ \max\left(a^-, b^+\right) \text{ if } \varphi_{p1}^0 < 1 \end{cases} \quad \frac{\partial d_{p1}^0}{\partial y} = \begin{cases} \max\left(c^+, d^-\right) \text{ if } \varphi_{p1}^0 > 1 \\ \max\left(c^-, d^+\right) \text{ if } \varphi_{p2}^0 < 1 \end{cases} \tag{27}$$

Similarly, $\frac{\partial d_{p2}^0}{\partial x}$ and $\frac{\partial d_{p2}^0}{\partial y}$ are treated the same as eq. (26) and eq. (27). In eq. (27), a, b, c, and d are defined as follows

$$a = \frac{\partial d_-^0}{\partial x} \approx \frac{\sum_{i=1}^{N_{face}} d_-^0 n_{i,x} A_i}{\Delta V}, \quad b = \frac{\partial d_+^0}{\partial x} \approx \frac{\sum_{i=1}^{N_{face}} d_+^0 n_{i,x} A_i}{\Delta V} \tag{28}$$

$$c = \frac{\partial d_-^0}{\partial y} \approx \frac{\sum_{i=1}^{N_{face}} d_-^0 n_{i,y} A_i}{\Delta V}, \quad d = \frac{\partial d_+^0}{\partial y} \approx \frac{\sum_{i=1}^{N_{face}} d_+^0 n_{i,y} A_i}{\Delta V} \tag{29}$$

$$d_-^o = d_-^0\big|_{p1} + \left.\frac{\partial d_-^0}{\partial x}\right|_{p1}(x_c - x_1) + \left.\frac{\partial d_-^0}{\partial y}\right|_{p1}(y_c - y_1)$$
$$d_+^0 = d_+^0\big|_{p2} + \left.\frac{\partial d_+^0}{\partial x}\right|_{p2}(x_c - x_2) + \left.\frac{\partial d_+^0}{\partial y}\right|_{p2}(y_c - y_2) \tag{30}$$

The value of d_{ij} away from the free surface is determined by solving eq. (23). Rewriting eq. (23) in its linearized form, the following expression is obtained:

$$sign\left(\varphi^0\right)\frac{\left(\nabla d^*\right)^{m-1}}{\left|\left(\nabla d^*\right)^{m-1}\right|}\cdot\left[\nabla\left(\Delta d\right)\right] = -sign\left(\varphi^0\right)\left(\left|\left(\nabla d^*\right)^{m-1}\right| - 1\right) \tag{31}$$

After numerical discretization, eq. (31) is written as an algebra equation as follows:

$$a_p \Delta d_p = \sum_{nb} a_{nb}\Delta d_{nb} + RHS_d \tag{32}$$

Coefficients of a_{nb} for nodal points P_1 and P_2 are

$$a_{nb,p1} = \max\left(-\frac{sign\left(\varphi^0\right)\dfrac{\nabla d^*}{\left|\nabla d^*\right|n_i A_i}}{\Delta V},\ 0\right) \quad \text{and} \quad a_{nb,p2} = \max\left(\frac{sign\left(\varphi^0\right)\dfrac{\nabla d^*}{\left|\nabla d^*\right|n_i A_i}}{\Delta V},\ 0\right).$$

Coefficient of a_p is $a_p = \sum_{nb} a_{nb}$; the RHS_d is given by $RHS_d = -sign\left(\varphi^0\right)\left(\left|\Delta d^*\right| - 1\right)$.

It is noted that $\left|\nabla d^*\right|$ can be obtained as follows:

$$\left|\nabla d^*\right| = \sqrt{\left(\frac{\partial d^*}{\partial x}\right)^2 + \left(\frac{\partial d^*}{\partial y}\right)^2} = \begin{cases} \sqrt{\max(a_+^2, b_-^2) + \max\left(c_+^2, d_-^2\right)} & \text{if } \varphi_{p1}^0 \geq 0 \\ \sqrt{\max(a_-^2, b_+^2) + \max\left(c_-^2, d_+^2\right)} & \text{if } \varphi_{p1}^0 < 0 \end{cases} \tag{33}$$

The subscripted coefficients in eq. (33) are obtained as follows:

$$\begin{aligned} &a_+ = \max(a, 0), a_- = \max(a, 0)\ b_+ = \max(b, 0), b_- = \min(b, 0) \\ &c_+ = \max(c, 0), c_- = \min(c, 0)\ d_+ = \max(d, 0), d_- = \min(d, 0) \end{aligned} \tag{34}$$

The regular coefficients shown above (i.e., a, b, c, and d) are obtained as follows:

$$a = \frac{\partial d_-^*}{\partial x} \approx \frac{\sum_{i=1}^{N_{face}} d_-^* n_{i,x} A_i}{\Delta V} \quad , \quad b = \frac{\partial d_+^*}{\partial x} \approx \frac{\sum_{i=1}^{N_{face}} d_+^* n_{i,x} A_i}{\Delta V} \tag{35}$$

$$c = \frac{\partial d_-^*}{\partial y} \approx \frac{\sum_{i=1}^{N_{face}} d_-^* n_{i,y} A_i}{\Delta V}, \quad d = \frac{\partial d_+^*}{\partial y} \approx \frac{\sum_{i=1}^{N_{face}} d_+^* n_{i,y} A_i}{\Delta V} \tag{36}$$

$$\begin{aligned} d_-^* &= d_{P1}^- + \frac{\partial d_{P1}^-}{\partial x}\left(x_c - x_1\right) + \frac{\partial d_{P1}^-}{\partial y}\left(y_c - y_1\right) \\ d_+^* &= d_{P2}^+ + \frac{\partial d_{P2}^+}{\partial x}\left(x_c - x_2\right) + \frac{\partial d_{P2}^+}{\partial y}\left(y_c - y_2\right) \end{aligned} \tag{37}$$

To solve eq. (32), the point Gauss-Seidel method is used again in the iterative procedure.

It takes substantial computer time to obtain velocity, pressure, and the level set function when the momentum equation, level set equation, etc. are solved. In this study, PC cluster was employed to perform the numerical computation. With 26 computer nodes and 1 control node, the PC cluster was made up of AMD X2 4400+ with 2GB memory and the control node was composed of AMD X2 3800+ with 2 GB memory. A gigabit switch was employed to connect each computer node, thus the message can transfer from one computer node to the other. For domain decomposition, METIS is applied to decompose the computational domain. METIS (Karypis 1998) is a set of programs for partitioning finite element meshes into graphics and reducing the storage and computational requirements of the sparse matrix factorization methods by up to an order of magnitude. The numerical simulation program is based on message passing interface (MPI) protocol to develop the current computational software.

In this study, the solution procedure adopted for coupled equations is summarized as follows:

1. specify the location of free surface at time $t = 0$;
2. calculate the normal distance for each nodal point from free surface;
3. calculate the gradient of velocity at cell center by Gauss' theorem;
4. specify the physical properties of fluid at each nodal point by eq. (5) and eq. (6);
5. solve the momentum equation and continuity equation at time $t + \Delta t$;
6. solve for level set equation using the velocities obtained from momentum equation;
7. perform re-initialization procedure by solving eq. (24) and eq. (33);
8. set $\varphi\left(\vec{r}, t + \Delta t\right) = d\left(\vec{r}\right)$;

9. repeat steps (3)-(8) for all time steps

4. Results and discussions

4.1 Numerical Validation

To evaluate the consistency of numerical solution, three different grid sets (100×100, 200×200, and 250×250) were used in this study. The liquid depth was chosen to be 0.21-m and the kinematic viscosities of liquid were 0.002 m^2/s and 0.0033 m^2/s. The dimension of tank is 1.0-m in breadth and 0.5-m in height. The excitation amplitude, A, is 0.1-m and the excitation frequency, ω, is 2.5132 rad/s. The rectangular tank was suddenly accelerated along horizontal direction; the horizontal acceleration of tank is expressed as follows:

$$\ddot{x}(t) = -A\omega^2 \sin(\omega t) \tag{38}$$

For the first case, the Reynolds number is 1,566 ($\mathrm{Re} = \frac{(b^3 g)^{1/2}}{\nu} = \frac{(1^3 \times 9.81)^{1/2}}{0.002} = 1,566.0$), based on the tank breadth, L; the boundary condition is no-slip on the wall. In Armenio's (1997) paper, the Semi-Implicit Marker and Cell (SIMAC) method was used to solve the Navier-Stokes equations in primitive variables on a non-uniform staggered grid by means of a finite difference scheme. In addition, the convection term was treated by using the second-order upwind scheme, and the diffusive term was solved by means of the implicit approximate factorization technique. The free surface was treated by using the massless particles which divide the domain of integration of full and empty cells as in a standard MAC method. However, in this paper, SIMPLE scheme was employed to calculate the flow field, and level set method was used to determine the free surface displacement. Fig. 6 shows the computational domain and grid distribution used in this study, and three grid distributions (100×100, 200×200, and 250×250) were used for the analyses, with the best distribution being 200×200 based on the free surface displacement obtained from the Armenio's result. For the first case with Reynolds number of 1,566 (as shown in Fig. 7 and Fig. 8), it is observed that the free surface displacement obtained from the present result is in good agreement with that obtained from the Armenio's result.

For the second case, the Reynolds number is 949.7 (using a liquid kinematic viscosity of 0.0033 m^2/s relative to 0.002 m^2/s used for the first case); moreover, boundary condition on the wall, density of liquid, density of air, mesh distribution, and total number of grids are the same as those of the pervious case (Re = 1,566). Using a kinematic viscosity of 0.0033 m^2/s, Fig. 9 shows the time histories of free surface displacements obtained from the Arimenio's method and from the present method; both results are in good agreement for this case too.

Nakayama and Washizu (1981) employed boundary element method to study the sloshing motion. The potential flow theory was used to build up the mathematical model for their research. Their study has now become the standard benchmark case for numerical simulation of sloshing motion. Three forced oscillation modes of the tank were studied by them – forced horizontal oscillation, forced vertical oscillation, and forced pitch oscillation. The work done in this paper followed their input data in order to validate our numerically simulated result. In their study, a two-dimensional rectangular tank was used, which was characterized by a tank breadth of 2b and liquid depth of h. The dimensions of tank were 2b = 0.9-m and h = 0.6-m. The excitation amplitude and excitation frequency in eq. (2) were chosen so that $A = 0.002$ m and ω =5.5 rad/s. The boundary condition at the wall was set to be free slip. As shown in Fig. 10, the time history of free surface displacement obtained from the present method is denoted by a solid line, and that obtained from the Nakayma's method is denoted by squares. It is seen that the time history of free surface displacements obtained from both methods are in good agreement.

Chen (2005) developed a numerical method to solve Navier-Stokes equations for two-dimensional sloshing motion. In his study, the coordinate transformation was employed to deal with complex free surface boundary. The Reynolds number used is 2,000. His study did not discuss fluid properties. The dimensions of tank are 0.9-m for the tank breadth and 0.6-m for the liquid depth. The horizontal acceleration of tank is the same as that used for the Nayakama's case. The excitation amplitude is 0.0033-m and excitation frequency is 9.7301 rad/s. The primary purpose of using this case is to discuss the time history of free surface when the excitation frequency is near the resonant frequency of the tank. Fig. 11 shows the predicted time history of free surface by the present method; Fig. 12 shows the predicted time history of free surface by Chen's method. It is observed that the maximum heights of free surface obtained from the present method and that obtained from the Chen's method are 0.18-m and 0.2-m, respectively. As shown in Fig. 11, the maximum height of free surface is observed during the first transition cycle, but the maximum height of free surface decays during the second and subsequent cycles until finally the fluid system approaches constant steady-state amplitude. For this validation case, the present result is in fair agreement with the Chen's result.

4.2 Parametric Studies

The variation of free surface displacement depends on various factors, such as excitation amplitude, excitation frequency, tank geometry, and viscosity of liquid. This paper performed parametric studies regarding excitation frequency, excitation amplitude, and viscosity of fluid.

4.2.1 Effect of excitation frequency on free surface displacement

Various free surface displacements in the tank were excited by a number of excitation frequencies. This paper presented several cases to study various excitation frequencies which have an impact on the free surface displacement. In this case, the excitation amplitude is 0.01-m; the kinematic viscosity of liquid is 0.001 m^2/s. The dimensions of tank and horizontal acceleration of tank are the same as those obtained from the Armenio's study. The liquid depth is 0.21-m and the resonant frequency of tank is expressed as follows:

$$\omega_n = \sqrt{\frac{g(2n+1)\pi}{L}\tanh\left(\frac{(2n+1)\pi}{L}h\right)} \tag{39}$$

Many numerical and experimental results showed that the free surface displacement depends on excitation frequency (Chen, 2005, Feng, 1997, Lohner, et al. 2006, Royon-Lebeaud, et al. 2007, Armenio, 1997). When the excitation frequency and resonant frequency are the same, then the free surface displacement reaches its maximum value. Table 1 shows the maximum free surface displacement as a function of the excitation frequency. Fig. 13 shows the maximum free surface displacements for various excitation frequencies. When the excitation frequency is 4.2212 rad/s, the maximum free surface displacement is 0.1211-m. It is noted that when the excitation frequency is different from the resonant frequency, then the maximum free surface displacement is less than 0.1211-m. It is observed that as excitation frequency increases, the free surface displacement increases, but when the excitation frequency is greater than the resonant frequency, the free surface displacement decreases. As shown in Fig. 13, the time history of free surface displacement changes drastically by an excitation frequency near the resonant frequency. As shown in Fig. 14, the maximum free surface displacement depends on the excitation frequency.

Fig. 15 shows the time history of free surface for various modes of oscillation. For the fundamental mode (n=0), the maximum free surface displacement is much larger than that of the other modes of oscillation. For the first mode (n=1), the free surface displacement is 0.059-m when t = 5.0 s. For the second mode (n=2), the free surface displacement is 0.05-m when t = 3.3 s. For the third mode (n=3), the free surface displacement is 0.043-m when t = 0.27 s. As mentioned above, as excitation frequency increases, the maximum free surface displacement occurs at an early time while the maximum free surface displacement decreases at a slightly later time. As can be seen from time history of free surface, the maximum free surface displacement occurs and then the free surface displacement approaches the constant steady-state amplitude. Fig. 16 shows the shape of the free surface displacement for various modes of frequency, and the standing waves are shown for the cases with n = 1, 2, 3, and 4, respectively.

4.2.2 Effect of liquid depth on free surface displacement

Eswaran et al. (2009) performed the experimental work and numerical evaluation to study the effect of liquid depth on free surface displacement. Chen (1999) developed a numerical algorithm to investigate the free surface displacements under various liquid depths. This section of the study was intended to develop a numerical method to evaluate the effect of liquid depth on free surface displacement. In eq. (4), the resonant frequency of the tank depends on the liquid depth inside the tank. At a specific excitation frequency, numerical tests were done to study the free surface displacements under various liquid depths. In this study, five different liquid depths – 0.1-m, 0.15-m, 0.20-m, 0.25-m, and 0.30-m – were used, as shown in Fig. 17. For the case with a liquid depth of 0.30-m, the excitation frequency and excitation amplitude were found to be 4.7168 rad/s and 0.01-m, respectively, by using eq. (4). Table 2 shows the resonant frequencies for the five liquid depths considered in this study. Fig. 17 shows that the free surface displacement is related to its corresponding liquid depth. At a specified liquid depth, as the excitation frequency is near the resonant frequency of the tank, then its free surface displacement reaches a maximum value (Chen, 1999). As mentioned above, the free surface displacement depends on its excitation frequency. As the liquid depth increases, the resonance frequency of the tank is gradually approaching its excitation frequency; thus, the free surface displacement increases with an increasing excitation frequency. Fig. 18 shows variation of the free surface displacement as a function of the changing liquid depth in the tank. As shown in Fig. 19, the free surface displacements have the same trends as those shown in Fig. 17. For Fig. 19 in conjunction with eq. (4), the excitation frequency was found to be 3.67909 rad/s at the liquid depth of 0.15 m. In addition, the maximum free surface displacement decreases as the liquid depth increases, as shown in Fig. 20. The reason for this is that when the liquid depth is rising, the resonant frequency of a liquid

depth is deviated from the excitation frequency; as a result, the free surface displacement decreases.

4.2.3 Effect of excitation amplitude on free surface displacement

Fig. 21 shows the free surface displacement as a function of excitation amplitude, and Fig. 22 shows the time history of free surface displacements for various excitation amplitudes. For the cases studied, the excitation frequency was assumed to be 5.5 rad/s; the free surface displacements were evaluated by the level set method for five excitation amplitudes of 0.005-m, 0.01-m, 0.015-m, 0.02-m, and 0.025-m, respectively. As shown in Fig. 22, the frequencies of occurrence of free surface displacements are the same for various excitation amplitudes. In addition, as shown in Fig. 21 for fixed excitation frequency of 5.5 rad/s, the free surface displacement is nearly linearly proportional to the excitation amplitude. In other words, as the excitation amplitude increases, the free surface displacement increases also. Because as the excitation amplitude increases, the kinetic energy of liquid also increases; as a result, the free surface displacement increases also.

4.2.4 Effect of various parameters on pressure

Due to the fact that the sloshing motion is caused by horizontal oscillation, the large liquid movement in a rectangular tank creates the localized impact pressure. The impact pressure on the wall of tank might cause the structural damage. This impact pressure is called slosh-induced dynamic pressure (Kim, 2004). This study specified various excitation frequencies to study the effect of excitation frequency on pressure. Fig. 23 shows the time history of pressures for various excitation frequencies – ranging from $\omega = 0.75\omega_o$ to $1.5\omega_o$, where ω_o is the resonant frequency of the tank in conjunction with its liquid depth of 0.21 m which is taken from Armenio (1997). When the tank moves in one direction, the liquid in the tank moves in an opposite direction so that the free surface rises on the adjacent sidewall. This phenomenon causes an abrupt increase in the impact pressure at the adjacent sidewall. Also shown in Fig. 23, the impact pressure is changed by the existence of the fluid flow in the system. When the free surface of liquid water rises on one side of the wall, the impact pressure suddenly increases. As shown in Figures 14(c) and 24(c), both the free surface displacement and the impact pressure change drastically for excitation frequency near the resonant frequency. It is noted that variations of both of these physical quantities are much reduced for the region where the excitation frequency is far away from the resonant frequency. Fig. 24 shows that the impact pressure at y = 0.05-m varies with liquid depth. As a result of an increase in liquid depth, both the impact pressure and its associated maximum impact pressure increase. In addition, at y = 0.05-m the impact pressure varies with its associated excitation amplitude, as shown in Fig. 25. Furthermore, at y = 0.05-m the excitation amplitude causes an increase in its free surface displacement so that the maximum impact pressure also increases.

5. Conclusions

In this study, the results obtained from the numerical methodology developed have been validated. The numerical methodology was based on (1) cell-centered pressure-based SIMPLE scheme used to solve the Navier-Stokes equations and (2) advection equation used in the Level Set Method. In addition, parametric studies have been carried out for parameters such as excitation frequency, excitation amplitude, impact pressure, and liquid depth. The following conclusions have been reached:

1. Numerically simulated results obtained in this study have been validated by published results obtained from Armenio (1997), Chen (2005), and Nakayama (1981). Good agreements have been achieved among the simulated results obtained in this paper compared to those obtained in the literature.
2. For a given excitation amplitude together with a liquid depth, the free surface displacement increases when the excitation frequency is less than the resonant frequency of the tank. However, the free surface displacement decreases when the excitation frequency is larger than the resonant frequency of tank. It is noted that the maximum free surface displacement is generated under the circumstance for which the excitation frequency approaches the resonant frequency.
3. For fixed excitation amplitude and excitation frequency, an increase in liquid depth cause free surface displacement to decrease. When the excitation frequency is approaching the resonant frequency, free surface displacement increases as the liquid depth increases.
4. The excitation amplitude and the excitation frequency have a substantial effect on the impact pressure on the wall of the tank under investigation.

References

Armenio, V. (1997) "An improved MAV method (SIMAC) for unsteady high-Reynolds free surface flows", Int. J. Numer. Meth. Fluids Vol. 24, pp. 185-214.

Biswal K.C., Bahattacharyya, S.K., and Sinha, P.K. (2006) “Non-linear sloshing in partially liquid filled

container with baffles", Int. J. Numer. Meth. Engng. Vol. 28, No. 6, pp. 317-337.
Chen, H. Huang, P.G. and LeBeau, R.P., (2005) "A cell centered pressure based method for two/three dimensional unstructured incompressible Navier-Stokes Solver", 43rd AIAA Aerospace Sciences Meeting and Exhibit; Reno, NV; USA; 10-13 Ja. 2005.
Chen, B. F. and Chiang H. W., (1999), "Complete 2D and fully nonlinear analysis of ideal fluid in tanks, J. Engng Mech., Vol. 125, No. 1, pp. 70-78.
Chen, B. F. and Nokes, R. (2005), "Time-independent finite difference analysis of fully non-linear and viscous fluid sloshing in a rectangular tank", J. Comput. Phys., Vol. 209, No. 1, pp. 47-81.
Chen, Y. G., Djidjeli, Price, W. G., (2009), "Numerical simulation of liquid sloshing phenomena in partially filled containers", Comput. Fluids, Vol. 38, No. 4, pp. 830-842.
Cho J. R. and Lee H. W. Lee, (2004) "Numerical study on liquid sloshing on baffled tank by nonlinear finite element method", Comput. Methods Appl. Mech. Engrg., Vol. 193, No. 23-26, pp. 2581-2598.
Colicchio, G. Landrini, M. and Chaplin, J. R., (2005), "Level set Computations of free surface Rotational flows", J. Fluids Engng. Vol. 127, No. 6, pp. 1111-1121.
Eswaran, M. Shaha, U. K., and Maity, D., (2009), "Effect of baffles on a partially filled cubic tank: Numerical simulation and Experimental validation", Comput. Struct., Vol. 87, No. 3-4, pp. 198-205.
Feng, Z. C., (1997), "Transient to traveling waves from standing waves in a rectangular container subjected to horizontal excitations", Phys. Rev. let., Vol. 79, No. 3, pp. 415-418.
Frandsen J. B. (2004), "Sloshing motions in excited tanks" J. Comput. Phys., Vol. 196, No. 1, pp. 53- 87.
Firouz-Abadi, R. D., (2008), "Haddadpour, H., Noorian, M. A., and Ghasemi, M., A 3D BEM model for liquid sloshing in baffled tank", Int. J. Numer. Meth. Engng, Vol. 76, No. 9, pp. 1419-1433.
Ferziger, J.H. and Peric, M. (2002), Computational method for Fluid Dynamics, Springer-Verlag .
Hamano, K., Murashige, S. and Hayami, K. (2003), "Boundary element simulation of large amplitude standing waves in vessels", Engineering Analysis with Boundary elements, Vol. 27, No. 6, pp. 565-574.
Hartmann, D. Meinke, M. Schroder, W., (2008), "Differential equation based constrained reinitialization for level set method", J. Comput. Phys, Vol. 227, No. 14, pp. 6821-6845.
Hirt C. W. and Nichols, B. D. (1981), "Volume of fluid (VOF) method for the dynamics of free Boundaries", J. Comput. Phys., Vol. 39, No. 1, pp. 201-225.
Iglesias A. S. Rojas, L. P. and Rodriguez, Z., (2004), "Simulation of anti-roll tanks and sloshing type problems with smoothed particle hydrodynamics", Ocean Engng, Vol. 31, No. 8-9, pp. 1169-1192.
Iglesias, A. S., Delorme, L. Rojas, L. P., and Perez, S. A., (2009), "A set of canonical problems in sloshing, Part I: Pressure field in forced roll−comparison between experimental results and SPH", Ocean Engng, Vol. 36, No. 2, pp. 168-178.
Karypis G. and Kumar, V., (1998) A software package for partitioning unstructured graphs, partitioning meshes, computing fill-reducing orderings of sparse matrices Version 4.0, URL: http://www.cs.umn.edu/~karypis
Kim, Y., Shin, Y. S. and Lee, H. Y., (2004) "Numerical study on slosh-induced impact pressures on three-dimensional prismatic tank", Appl. Ocean Res., Vol. 26, No. 5, pp. 213-226.
Liu, D. and Lin, P., (2008), "A numerical simulation study of three dimensional liquid sloshing in tanks, J. Comput. Phys., Vol. 227, No. 8, pp. 3921-3939.
Lohner, R., Yang, C., and Onate, E., (2006), "On the simulation of flows with violent free surface motion", Comput. Methods Appl. Mech. Engrg., Vol. 195, No. 41-43, pp. 5597-5620.
Marchandise, E. and Remacle, J. F., (2006), "A stabilized finite element method using a discontinuous level set approach for solving two phase incompressible flows", J. comp. Phys. Vol. 219, No. 2, pp. 780-800.
Nakayama, T. and Washizu, K., (1981), "The boundary element method applied to the analysis of two-dimensional nonlinear sloshing problems", Int. J. Numer. Meth. Engng., Vol. 17, No. 11, pp. 1631-1646.
Nakayama, T. and Washizu, K., (1980), "Nonlinear analysis of liquid motion in a container subjected to forced pitching oscillation", Int. J. Numer. Meth. Engng., Vol. 15, No. 8, pp. 1207-1220.
Noh, W. F. and Woodward, P., (1976), "SLIC (Simple Line Interface Calculation)", Lecture Notes in Physics, Vol. 59, pp. 330-340.

Osher, S. and Sethian J. A., (1998), "Fronts propagating with Curvature-dependent speed: algorithm based on Hamiltion-Jacobi Formulations", J. Comput. Phys., Vol. 79, No. 1, pp. 12-49.

Okamoto, T. and Kawahara, M., (1990), "Two dimensional sloshing analysis by Lagrangian finite element method", Int. J. Numer. Meth. Fluids, Vol. 11, No. 5, pp. 453-477.

Ramaswamy, B., Kawahara, M. and Nakayama, T., (1986), "Lagrangian finite element method for the analysis of two-dimensional sloshing problems", Int. J. Numer. Meth. Fluids, Vol, 6, No. 9, pp. 659-670.

Rhee, S. H., (2005), "Unstructured grid based Reynolds-averaged Navier-Stokes method for Liqiud tank sloshing", J. of Fluid Engineering, Vol. 127, No. 3, pp. 405-627.

Royon-Lebeaud, A., Hopfinger, E. J. and Cartellier, A., (2007), "Liquid sloshing and wave breaking in circular and square-base cylindrical containers", J. Fluid Mech., Vol. 577, pp. 467-494.

Russo, M. and Smereka, P., (2000), "A remark on computing Distance functions", J. comput. Phys., Vol. 163, No. 1, pp. 51-67.

Rhie, C. M. and Chow, W. L., (1983), "Numerical study of the turbulent flow past an airfoil with trailing edge separation", AIAA J. Vol. 21, No. 3, pp. 1525-1532.

Sriram, V. Sannasiraj, S. A., Sundar, V., (2006), "Numerical simulation of 2D sloshing waves due to horizontal and vertical random excitation", Appl. Ocean Res., Vol. 28, No. 1, pp. 19-32.

Wu, G. X., Ma. Q, W, and Taylor R. E., (1998), "Numerical simulation of sloshing waves in a 3D tank based on a finite element method", Appl. Ocean Res. Vol. 20, No. 6, pp. 337-355.

Wang C. Z. and Khoo, B. C., (2005), "Finite element analysis of two-dimensional nonlinear sloshing problems in random excitations", Ocean Engng, Vol. 32, No. 2, pp. 107-133.

Youngs, D. L., (1982), "Time-dependent multi-material flow with large fluid distortion", Numerical Methods for Fluids Dynamics, pp. 273-285.

Yue W. Lin C. L. and Patel V. C., (2003), "Numerical simulation of unsteady multidimensional free surface motions by level set method", Int. J. Numer. Meth. Fluids., Vol. 42, No. 8, pp. 853-884.

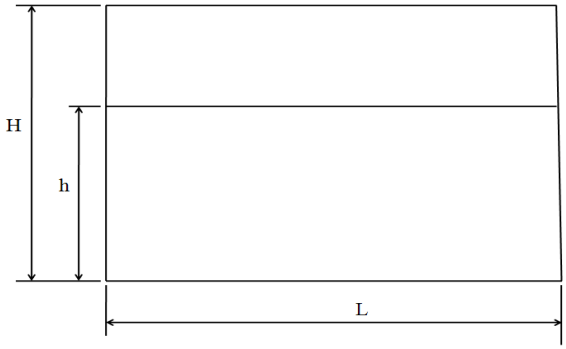

Figure 1. Dimension of tank

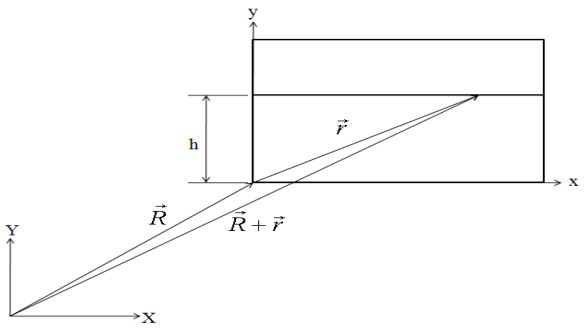

Figure 2. Non-inertia reference frame for 2-D tank

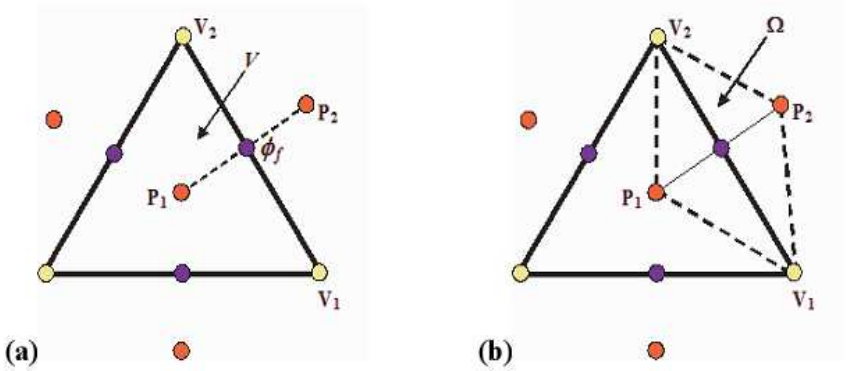

Figure 3. Schematic diagrams of integration areas: (a) convection fluxes and (b) diffusive fluxes

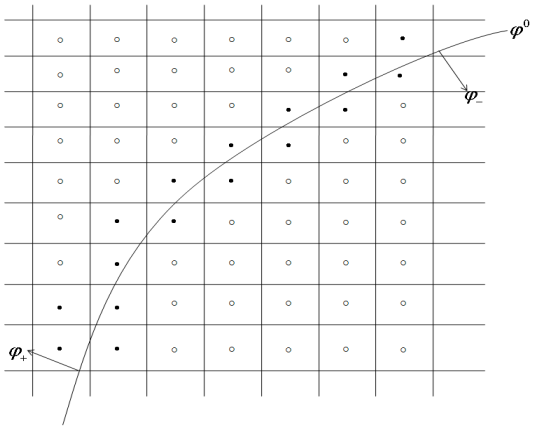

Figure 4. φ^0 is free surface; nodal points near free surface are denoted as black points; small circular points are nodal points away from free surface

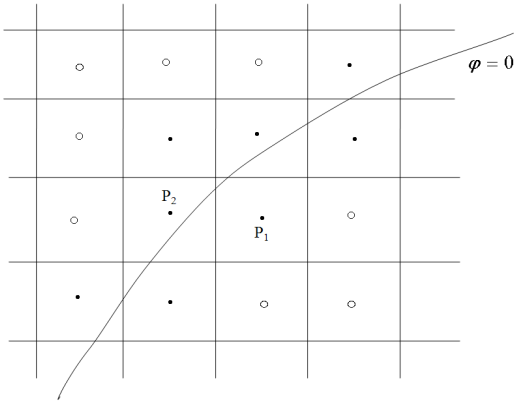

Figure 5. d_{ij} on the P_1 and P_2 obtained from eq. (24)

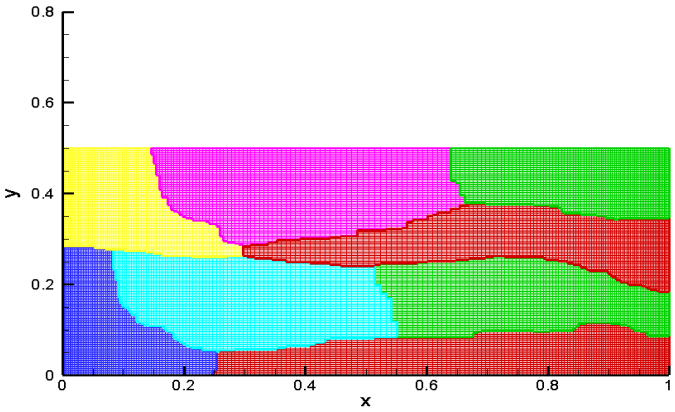

Figure 6. Computational domains and grid distributions

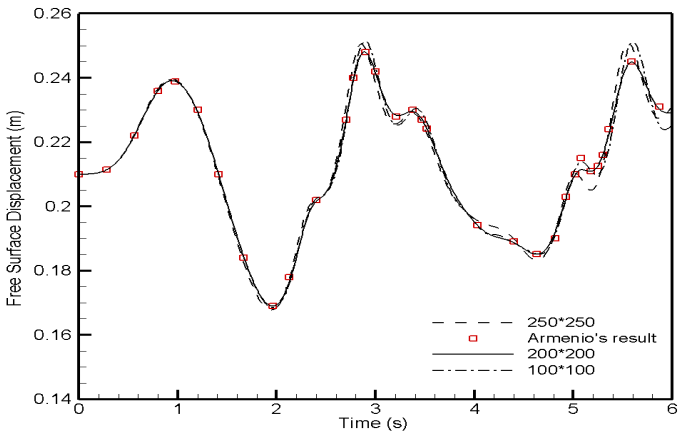

Figure 7. Free surface displacements versus time at x = 0.25 m for three different meshes

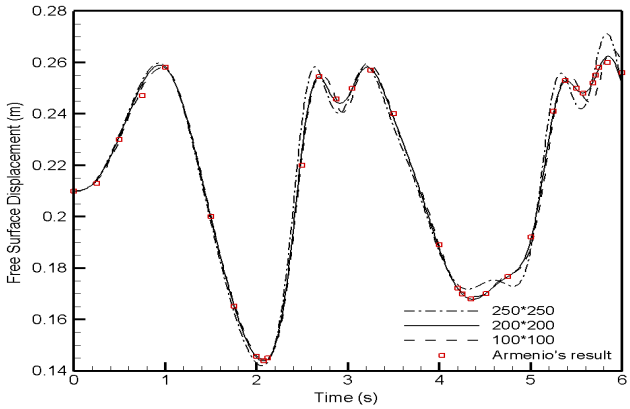

Figure 8. Free surface displacements (for three different meshes) versus time at wall on the left-hand side

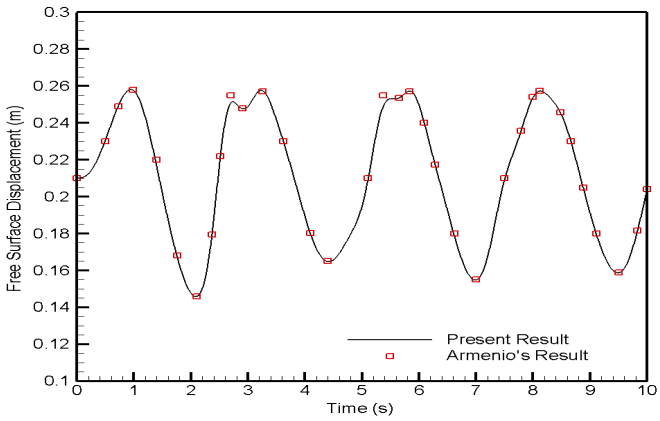

Fig. 9 Heights of free surface displacement (at x = 0.25 m) obtained from the present and Armenio's results

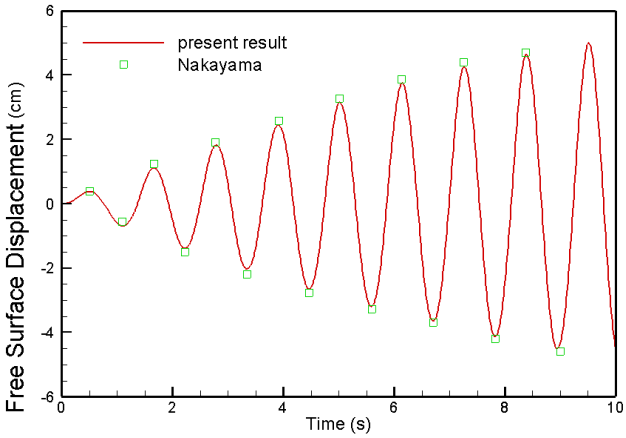

Figure. 10 Heights of free surface displacement (at the left-hand side of wall) obtained from the present and Nakayama's results

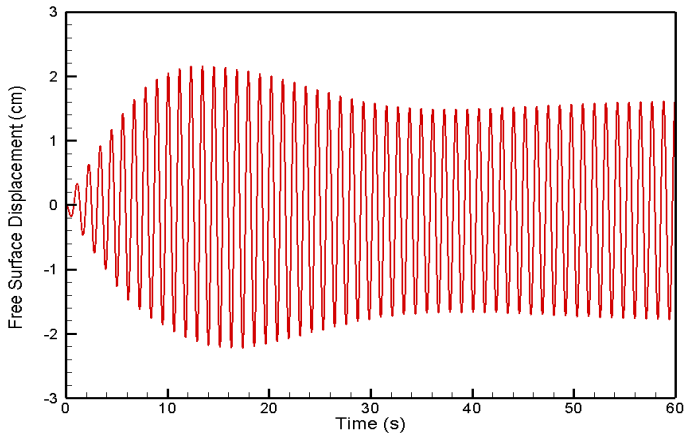

Figure 11. Predicted height of free surface displacement obtained from the level set method

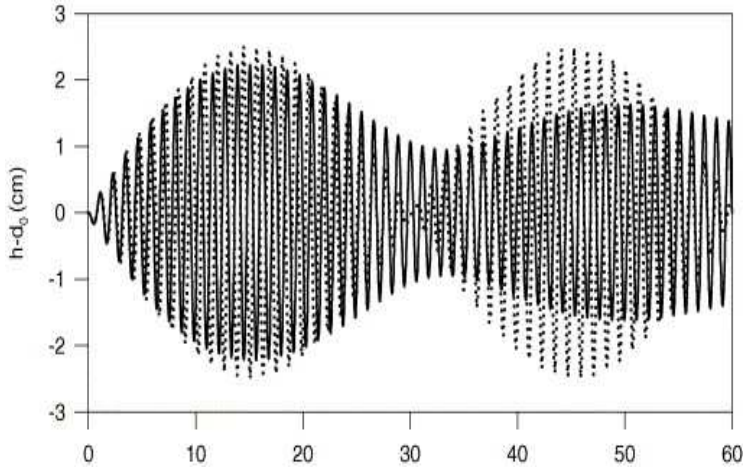

Figure 12. Predicted height of free surface displacement obtained from Chen's (2005) method

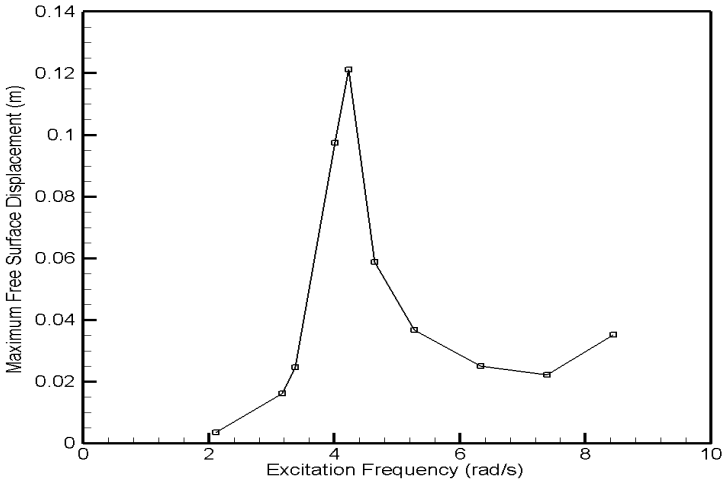

Figure 13. Free surface displacement versus excitation frequency

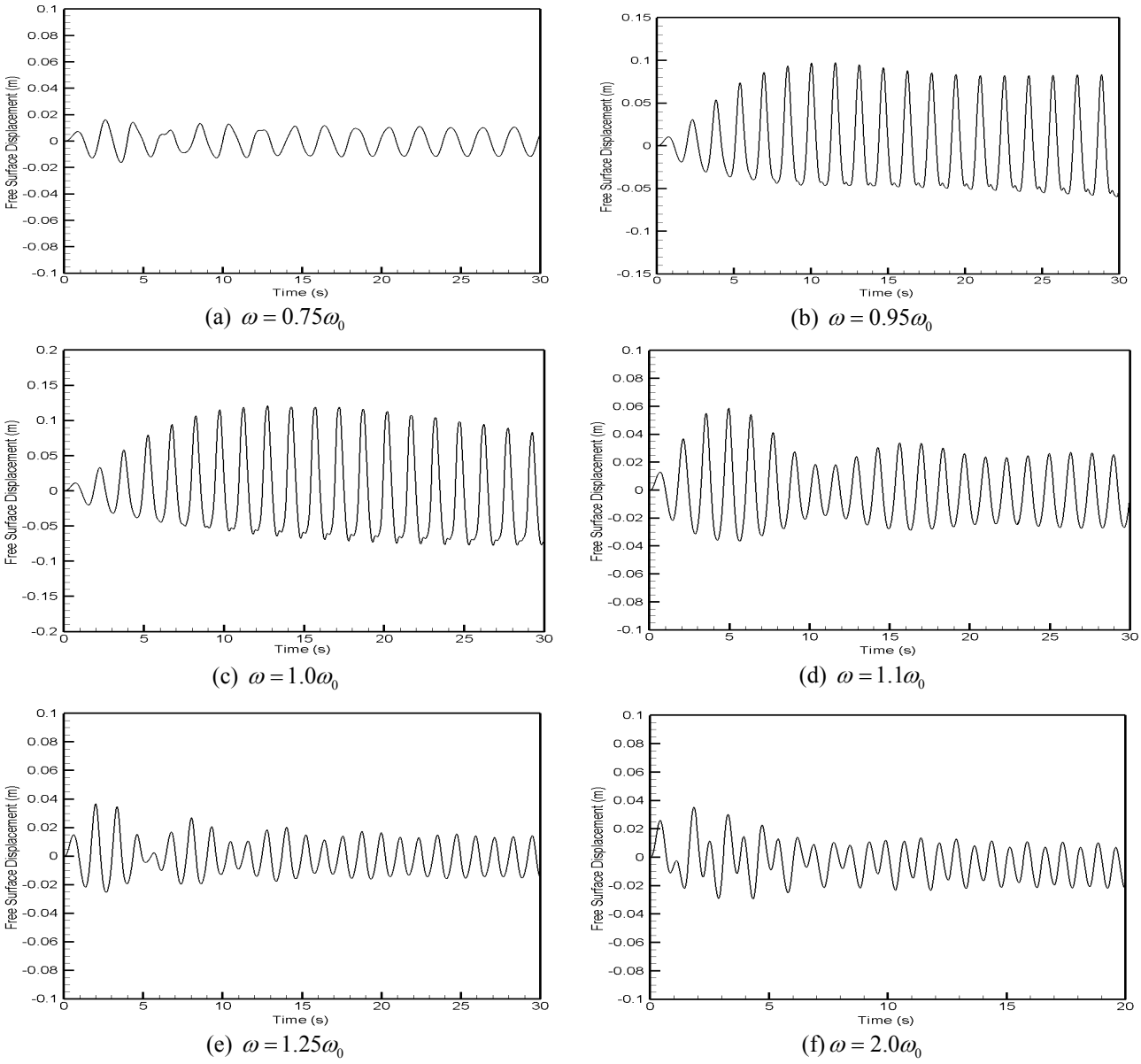

(a) $\omega = 0.75\omega_0$ (b) $\omega = 0.95\omega_0$

(c) $\omega = 1.0\omega_0$ (d) $\omega = 1.1\omega_0$

(e) $\omega = 1.25\omega_0$ (f) $\omega = 2.0\omega_0$

Fig. 14 Time histories of free surface displacement for various excitation frequencies

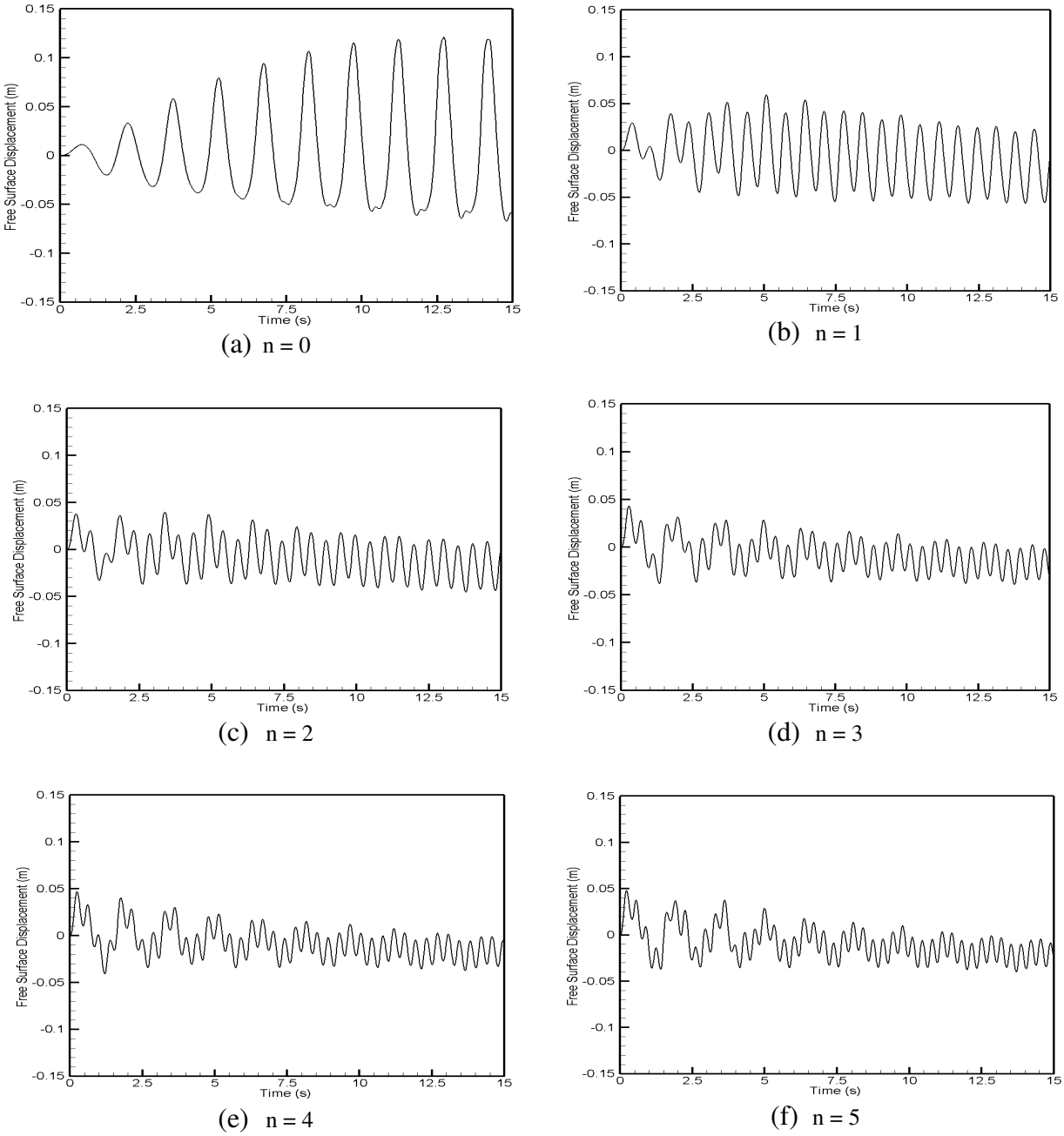

Figure 15. Time histories of free surface displacement at various modes of frequency

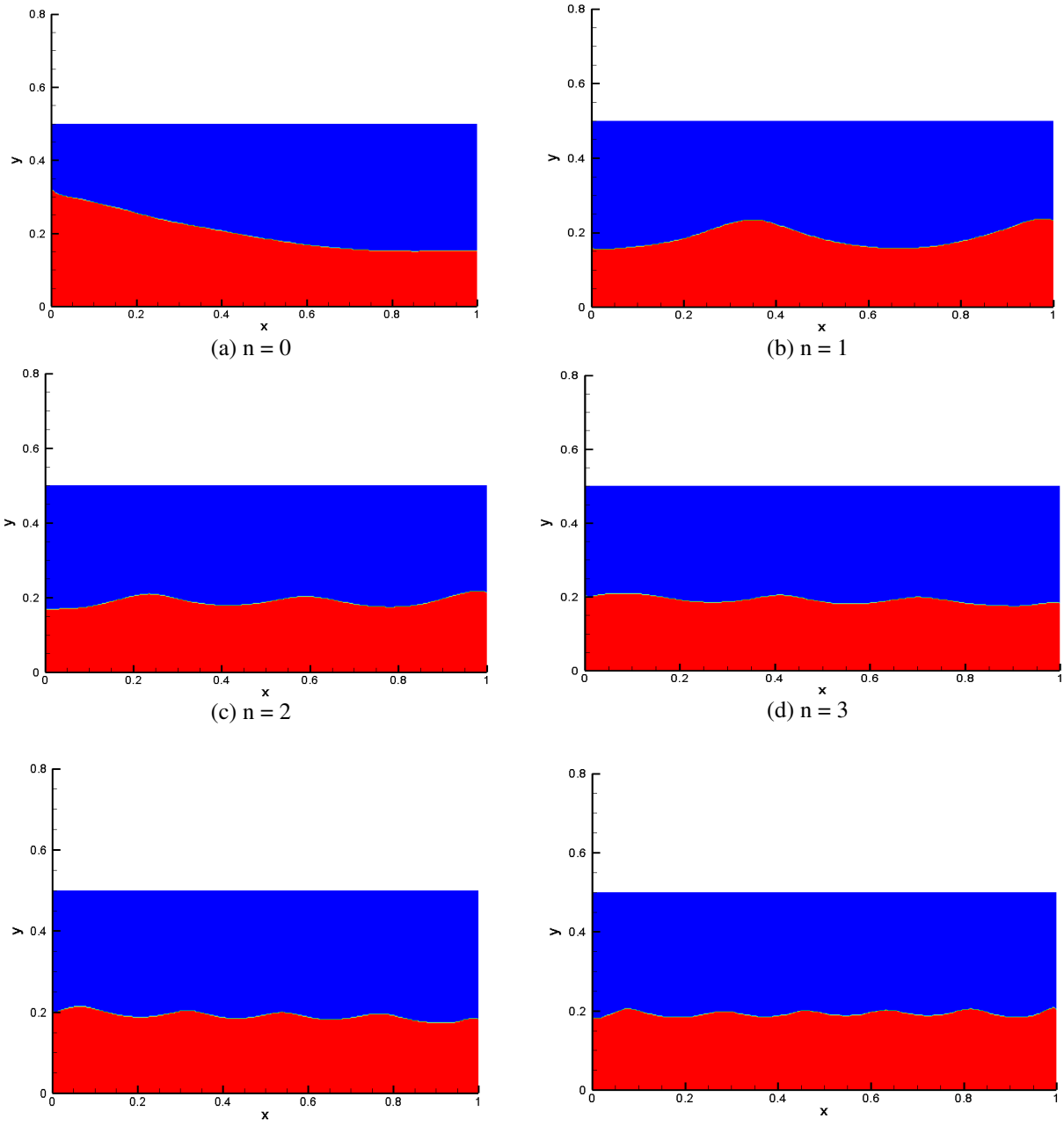

(a) n = 0 (b) n = 1

(c) n = 2 (d) n = 3

(e) n = 4 (f) n = 5

Figure 16. Shapes of free surface at various modes of frequency

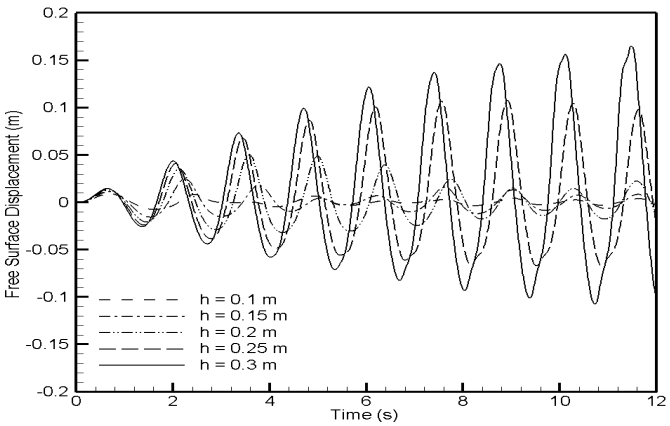

Figure 17. Time histories of free surface displacement for various fluid depths

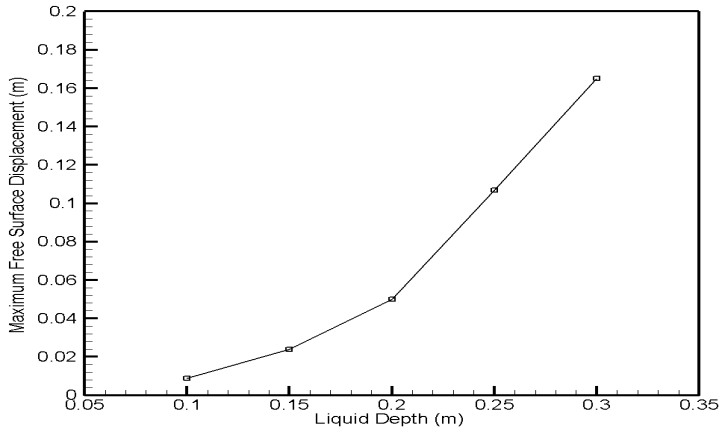

Figure 13. Elevation of maximum free surface displacement versus filled fluid depth

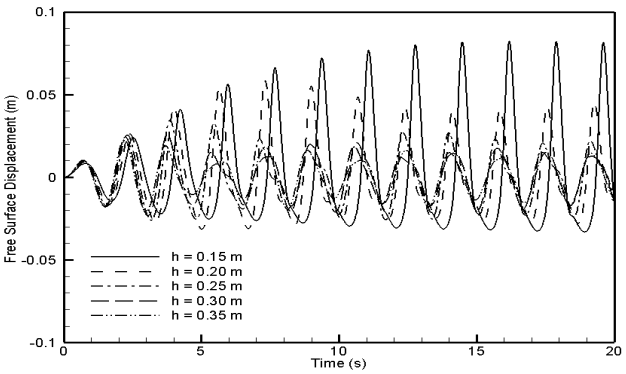

Figure 19. Time histories of free surface displacement for various fluid depths

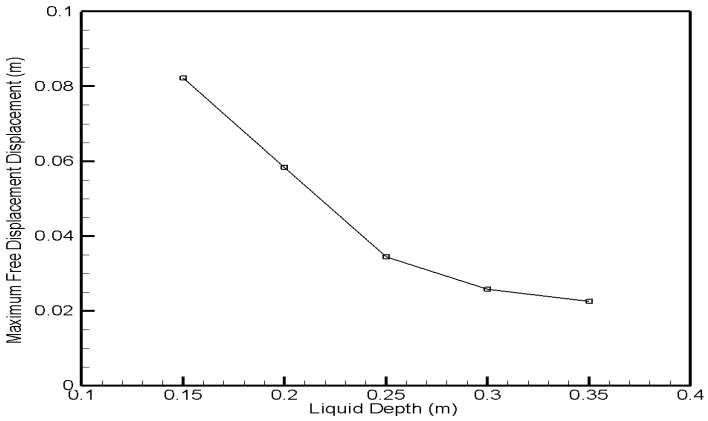

Figure 20. Maximum free surface displacement versus liquid depth

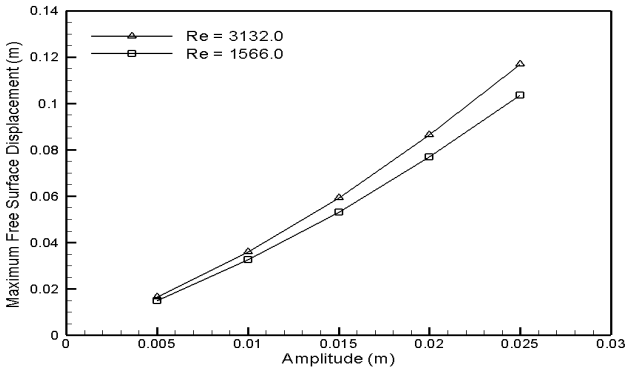

Figure 21. Maximum free surface displacement versus excitation amplitude

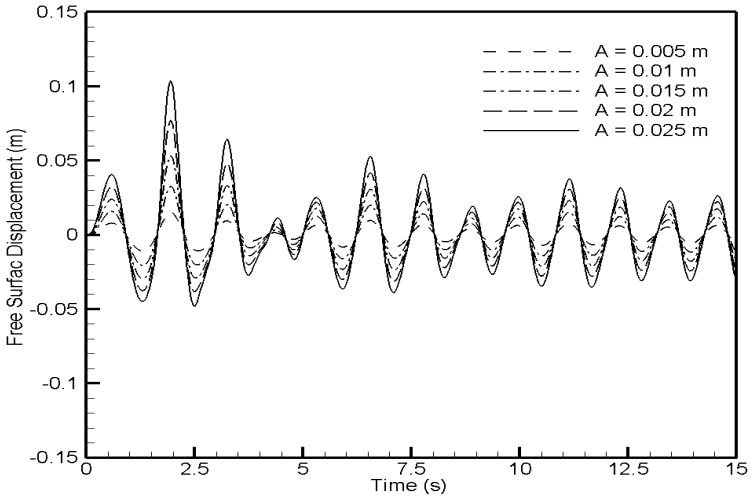

Figure 22. Time histories of free surface displacement for various excitation amplitudes

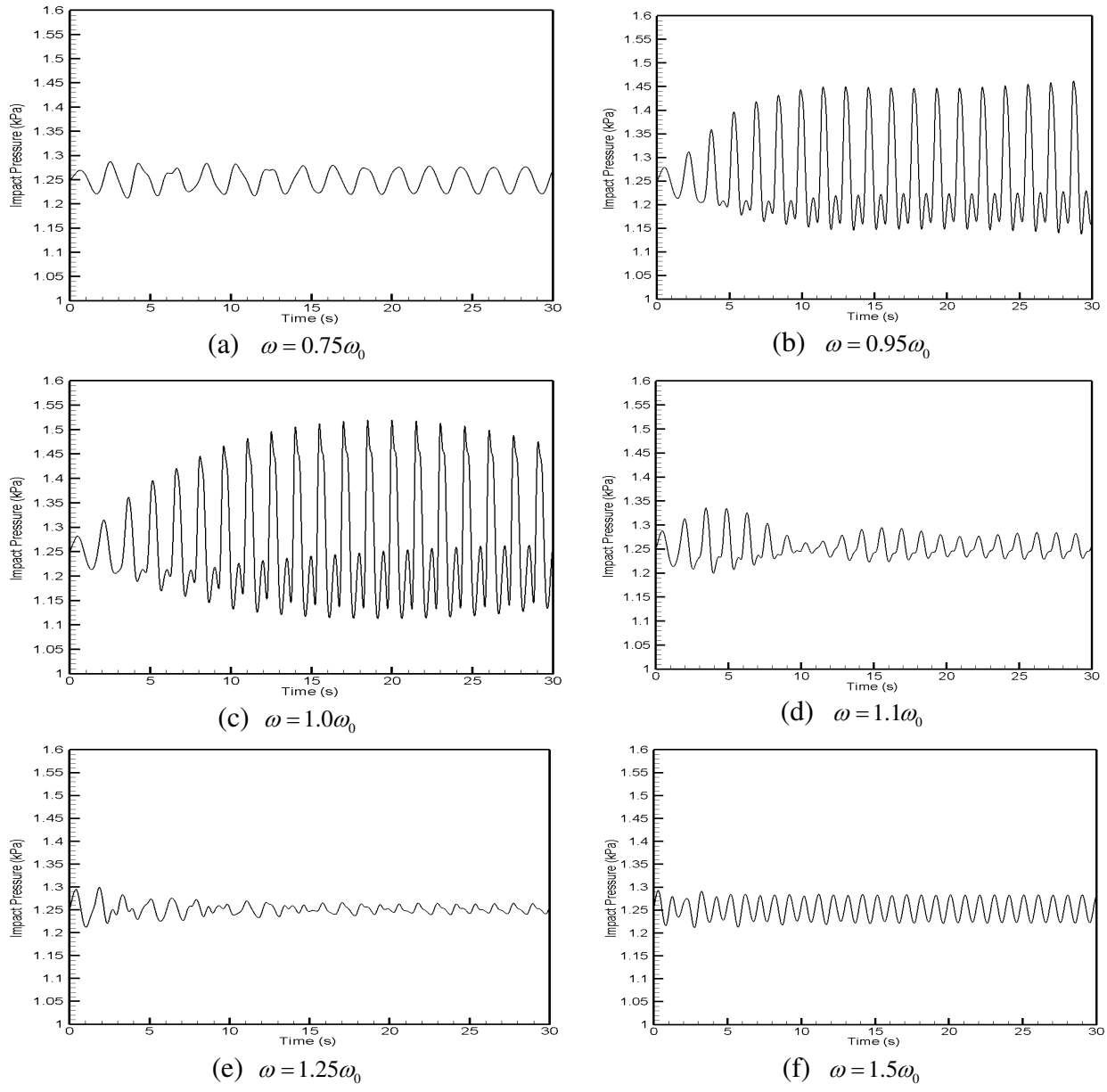

Figure 23. Time histories of impact pressure on the left-hand side of wall for various excitation frequencies

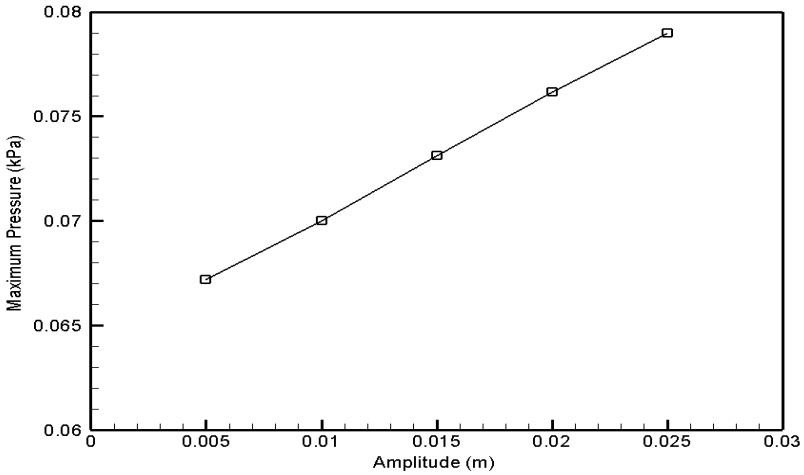

Figure 24. Maximum impact pressure versus liquid depth at y = 0.05 m

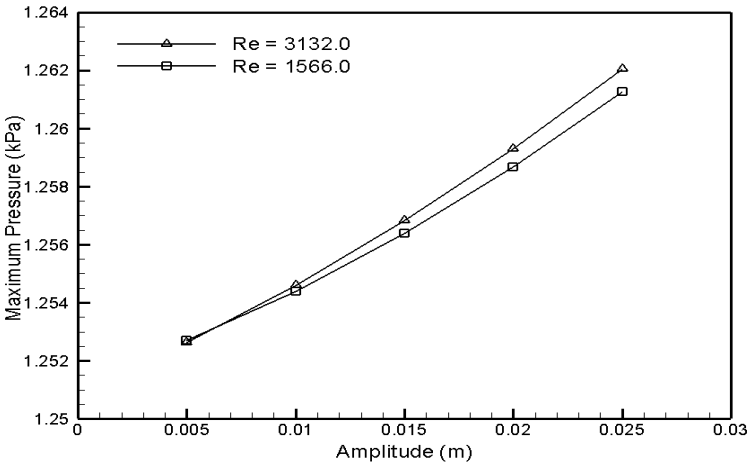

Figure 25. Maximum impact pressures (Re = 1566 and 3132) at y = 0.05 m for various excitation amplitudes

Table 1. Predicted maximum free surface displacements for various excitation frequencies

Excitation frequency (rad/s)	Non-dimensional excitation frequency	Maximum free surface displacement (m)
2.1106	0.6739	0.00346
3.1659	1.0108	0.01619
3.3769	1.0782	0.02463
4.0101	1.2804	0.09736
4.2212	1.3477	0.12117
4.6433	1.4825	0.05869
5.2765	1.6847	0.03668
6.3318	2.0216	0.02508
7.3871	2.3589	0.02215
8.4424	2.6955	0.03525

Table 2. Predicted maximum free surface displacements for various liquid depths

Liquid depth (m)	Resonant frequency (rad/s)	Maximum free surface displacement (m)
0.1	3.0620	0.0087
0.15	3.6791	0.0240
0.20	4.1428	0.050
0.25	4.4957	0.107
0.30	4.7638	0.165